Ecological Indicators 129 (2021) 107953

Contents lists available at ScienceDirect

Ecological Indicators

journal homepage: www.elsevier.com/locate/ecolind

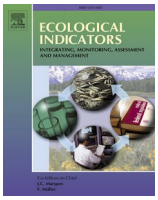

Soil drying weakens the positive effect of climate factors on global gross primary production

Huan Chen [a,d,f], Xiaoyong Bai [a,b,e,*], Yangbing Li [f], Qin Li [a], Luhua Wu [a,c,e], Fei Chen [a,d], Chaojun Li [a,c,e], Yuanhong Deng [a], Huipeng Xi [a,c,e], Chen Ran [a,d,f], Xuling Luo [a,d,f], Min Liu [a,d,f]

[a] State Key Laboratory of Environmental Geochemistry, Institute of Geochemistry, Chinese Academy of Sciences, Guiyang 550081, Guizhou Province, China
[b] CAS Center for Excellence in Quaternary Science and Global Change, Xi'an 710061, Shanxi Province, China
[c] University of Chinese Academy of Sciences, Beijing 100049, China
[d] Puding Karst Ecosystem Observation and Research Station, Chinese Academy of Sciences, Puding 562100, Guizhou Province, China
[e] Guizhou Provincial Key Laboratory of Geographic State Monitoring of Watershed, Guizhou Education University, Guiyang 550018, China
[f] School of Geography and Environmental Sciences, Guizhou Normal University, Guiyang 550001, China

ARTICLE INFO

Keywords:
GPP
Soil drying
Climate factors
Relative contribution
Global change

ABSTRACT

Global warming and the fertilization effect of carbon dioxide (CO_2) have led to a general increase in gross primary production (GPP). Although soil drying (SD) may limit this increase, its limiting effect has not been confirmed and quantified. Hence, we evaluated the impact of SD and climate factors on GPP. From 1997 to 2017, GPP showed a slight downward trend but began to rise after 2011. In SD zones, 19% of the GPP change was attributed to SD, and CO_2 concentration in climate factors was the climate factor that contributed the most (24%) and accounted for the main control area (9%). Surprisingly, the negative contribution of SD to GPP offset 35% of the positive contribution area of the climate factors. In addition, SD and climate factors explained 1% and 23% of the GPP increase, respectively, but in areas where GPP decreased, the SD area exceeded that of climate factors by 1.2 times, further highlighting the importance of SD in the GPP drive mechanism. Compared with previous studies, we further quantified the contribution of SD and climate factors to GPP, which improved our understanding of the global pattern of total carbon absorption and its response to SD and climate factors.

1. Introduction

The gross primary production (GPP) of terrestrial vegetation is the first step for atmospheric carbon dioxide (CO_2) to enter the biosphere (Zhang et al., 2017). It not only plays a key role in driving the global carbon cycle (Houghton, 2007) but also provides the necessary material and energy basis for almost all ecosystems (Beer et al., 2010) and is sensitive to changes in climate and environmental elements (Nemani, 2003). Therefore, understanding the relative impact of climatic and environmental factors on GPP changes is important for the reliable prediction of future feedback between the ecosystem and the atmosphere.

It is impossible, however, to observe GPP directly (Ma et al., 2015; Sun et al., 2018). Therefore, scholars have developed multiple sets of ecological process models to simulate GPP from different perspectives, such as ground, atmospheric, and space observations (Anav et al., 2015), which are used to discuss the impact of climate and environmental factors on GPP changes under different spatial scales, and it gradually is recognized that CO_2 concentration may be the most important factor driving the growth of global GPP since 1900 (Haverd et al., 2020; Schimel et al., 2015). Zhu et al. found, however, that the closure of vegetation stomata caused by elevated CO_2 concentration would weaken its own fertilization effect (Zhu et al., 2017). In addition, Wang et al. found through simulations that the increase in N deposition and the decrease in soil moisture (SM) also may weaken the positive impact of CO_2 in some arid areas (Wang et al., 2020b), whereas Reichstein et al. found that GPP is more sensitive to the continuous deficit of SM than evapotranspiration (Reichstein et al., 2002), these studies indicate that the effects of soil drying (SD) (Koster et al., 2004; Veldkamp et al., 2016) (SD represents the area where the Theil–Sen slope of SM is < 0) and N deposition on the carbon sink effect of vegetation also cannot be ignored (Arora et al., 2013). Under the background of current global warming, increasing of nitrogen deposition (ND) (Kanakidou et al., 2016) and CO_2 concentrations (Schimel et al., 2015), whereas decreasing of SM (Cai

* Corresponding author at: State Key Laboratory of Environmental Geochemistry, Institute of Geochemistry, Chinese Academy of Sciences, China.
E-mail address: baixiaoyong@vip.skleg.cn (X. Bai).

https://doi.org/10.1016/j.ecolind.2021.107953
Received 19 April 2021; Received in revised form 28 June 2021; Accepted 4 July 2021
Available online 9 July 2021

et al., 2009; Liu et al., 2021; Deng et al., 2020a) are gradually being recognized, however, research about a simultaneous assessment of the comprehensive effects of CO_2 concentration, ND, and SM on GPP on a global scale over recent years is still less.

In addition, the influence of precipitation (PRE) and temperature (TEM) on GPP has always been a research hotspot (Zhang et al., 2016, 2014; GIFFORD, 1995; Sun et al., 2019), but the temporal and spatial heterogeneity of the impact of PRE and TEM on GPP is becoming more and more complex and difficult to predict under the current global warming background. For example, in the tropical grassland ecosystem, the PRE significantly promotes the growth of vegetation (Knapp, 2001; Huxman et al., 2004), whereas in tropical rainforest areas, when the average annual PRE exceeds 3,000 mm/yr, the productivity of vegetation begins to show a downward trend (Schuur, 2003; Del Grosso et al., 2008). For TEM, previous studies have shown that rising TEM also will increase global GPP (Luo, 2007); however, the decrease in SM caused by rising TEM will exacerbate the drought stress effect (Liu et al., 2019a). Therefore, the phenomenon that GPP decreases with increasing TEM also has been widely reported (Ciais et al., 2005; Saleska et al., 2007). Recent simulation results for extreme climates indicate that global warming will limit the positive effects of extreme PRE (Wang et al., 2021), whereas site-based simulation studies have shown that the reduction in soil water supply caused by warming may offset some of the positive effects of TEM (Liu et al., 2019a). No research has quantified the weakening effect of SM reduction on PRE, TEM, and other factors on a global scale.

This study effectively distinguished and quantified the impact of SD and climate factors on changes in primary productivity. From 1997 to 2017, in our study, we considered SM and climate factors as evaluation indicators, among which the climate factors included PRE, TEM, ND, and CO_2 emission concentration. Then, combined with partial correlation and linear regression analysis, we quantitatively evaluated the contribution of SM and climate factors to GPP. Finally, according to the complexity and cross-effects of the driving factors, we determined the magnitude and area of offsetting in GPP caused by SD and evaluated the contribution rate of SD and climate factors to GPP. This enabled us to (1) understand the magnitude, spatial pattern, and dynamic trends of global terrestrial GPP from 1997 to 2017; (2) quantify the impact of SD and climate factors on GPP changes; (3) determine how much of the positive effect of climate factors on GPP has been offset by SD; and (4) determine the main control area of SD and climate factors to GPP. This research improved our understanding of the contribution of SD and climate factors to the primary productivity of vegetation in the context of global change and identified the impact of the joint action of the two factors on GPP. This research has important scientific significance for the study of global vegetation carbon absorption and mitigation of climate warming.

2. Materials and methods

2.1. Materials

2.1.1. GPP dataset

We based the GPP data on photosynthetically active radiation (PAR), normalized vegetation index, TEM, evaporation, and net radiation drive in the Global Land Surface Satellite and calculated the GPP with production efficiency models using input from remote sensing products (http://www.glass.umd.edu/Download.html (sensor: AVHRR)). The structure, climate input, and parameterization of the model have been detailed in Liang et al. (2013). Production efficiency principles have been widely used, including the Carnegie–Ames–Stanford approach (Potter et al., 1993), the simple biosphere model (Sellers et al., 1986), and the global production efficiency model ((Prince and Goward 1995). The MODIS photosynthesis and net primary production product algorithm (MOD17) is also based on this model (Zhao et al., 2006), and all of these models require input of PAR data (Liang et al., 2013). GPP data have a spatial resolution of 0.05 degree and a time resolution of 8 days. These data have been proven to be of high quality and accuracy and are widely used (Wang et al., 2020a; Zheng et al., 2018; Yu et al., 2018a, 2018b).

2.1.2. Climate factors dataset

The climate dataset for this study included PRE, TEM, CO_2 concentration, and ND data. Specifically, the CO_2 emissions concentration data from 1997 to 2017 were provided by the European Commission Joint Research Center and the Dutch Environmental Assessment Agency (https://edgar.jrc.ec.europa.eu/), with a spatial resolution of 0.1 degree. Compared with EDGAR v4.3.2, the new time profile included the calculation of monthly emissions (Crippa et al., 2020). The new space agent is used to allocate population-related emissions based on global human settlement layer products (Pesaresi et al., 2019) and used the PRE and TEM data from the CRUTS v4.03 version (http://www.cru.uea.ac.uk/data) released by the Climate Research Institute (CRU) of the University of East Anglia, it is derived by interpolating monthly climate anomalies in weather station observation data, covering the years from 1901 to 2018, with a resolution of 0.5 degree. The accuracy of the CRU data has been reliably verified in related studies at the global scale and other levels (Harris et al., 2020).

2.1.3. Related auxiliary dataset for nitrogen deposition

We simulated long-term series of atmospheric ND data using a linear regression model, as shown in formula (1), in which the atmospheric ND site data were simulated by GEOS-Chem, involving the four time periods of 1984–1986, 1994–1996, 2004–2006, and 2014–2016, including each grid unit each year. Among them, the site data contained the spatial explicit information of dry, wet, and total (dry + wet) ND for each grid unit each year (https://conservancy.umn.edu/handle) (Ackerman et al., 2018). Surface temperature came from the MOD11 satellite, the spatial resolution was 5.5 km, and its temporal resolution was once a month (Wan et al., 2015). We obtained PRE data from CRUTS v4.03 and calculated relative humidity according to the model (see Method 2.2.2). Wind speed was provided by the Goddard Earth Science Data and Information Service Center and was a data product of GLDAS-2. This version was updated once a month from 2000 to the present, with a spatial resolution of 0.25 degree. Nitrogen dioxide (NO_2) column concentration was based on satellite observation results, and using differential optical absorption spectroscopy technology and the Royal Netherlands Meteorological Institute combined modeling/retrieval/assimilation method, the data came from three sensors: GOME (Global Ozone Monitoring Experiment), SCIAMACHY (Scanning Imaging Absorption Spectrometer for Atmospheric Cartography), and GOME-2 (METOP-A) (Global Ozone Monitoring Experiment-2) (http://www.temis.nl/airpollution/no2.html).

2.1.4. Soil moisture dataset

This study uses 0–10 cm SM data, the GLDAS–2.1 Noah dataset provided by NASA Goddard Geoscience Data and Information Service Center (https://ldas.gsfc.nasa.gov/gldas/). The data set contains four layers of SM data with their depths of 0–10, 10–40, 40–100, and 100–200 cm, respectively, with a spatial resolution of 0.25 degree. The main noun abbreviations used in the paper are shown in the table below (Table 1).

Table 1
The meaning of the acronyms and symbols.

Acronyms	Full name	Acronyms	Full name
GPP	Gross primary production	ND	Nitrogen deposition
SM	Soil moisture	PAR	Photosynthetically active radiation
SD	Soil drying	CRU	Climate Research Institute
PRE	Precipitation	MK	Mann–Kendall
TEM	Temperature	/	/

2.2. Methods

2.2.1. Nitrogen deposition model

Previous studies have shown that ND is affected by human activities and meteorological factors (Lu et al., 2013; Walcek et al., 1986; Wesely, 2007). Therefore, in order to be able to quickly and efficiently simulate and obtain global high-temporal-spatial resolution ND, we focused on the linear regression model published by Lu et al. (2013). This algorithm is based on the linear correlation between ND, meteorological elements and NO_2 concentration, etc., and can simulate the distribution of ND more accurately and quickly, and the algorithm has been cited by many studies (John et al., 2020; Chen et al., 2019b). Based on R, we referred to the model of Lu et al. (2013) and establishing a pixel-by-pixel spatial linear regression model based on the existing ND data and NO_2 column concentration, PRE, TEM, relative humidity, wind speed, etc. Then, we estimated the long-term series of ND data based on the model and its parameter inversion. The reference formula of the model is as follows:

$$N_{dep} = a_0 t + a_1 p + a_2 h + a_3 w + a_4 C + b$$

where a_0, a_1, a_2, a_3, a_4, and b are the regression coefficients of the linear equation; N_{dep} is the atmospheric nitrogen deposition, unit: g N/m^2; t is the surface temperature; p is the precipitation; h is the relative humidity; w is the wind speed; C is the NO_2 column concentration.

2.2.2. Relative humidity estimation model

The relative humidity of air is defined as the ratio of the vapor pressure of air to its saturation vapor pressure (Castellví et al., 1996), and it has a significant impact on the sedimentation rate and conversion rate of organic nitrogen and inorganic nitrogen (Brem et al., 2015). It is a dimensionless value and it is given as a percentage from 0 to 100, and the general formula for calculating relative humidity is as follows (Hardwick et al., 2015):

$$RH = \frac{E}{E_S} \times 100$$

Where E is the actual water vapour partial pressure in air, and Es is the saturated vapor pressure. For the actual water vapour partial pressure E, it is a key parameter for calculating the specific humidity in the air (Berg et al., 2016; McKinnon et al., 2021), some scholars deduced the formula for calculating E by combining the known specific humidity with the surface pressure as follows (Lagler et al., 2013), and this formula has been widely cited (Jolly et al., 2015) (equation 3).

$$E = q \times \frac{p}{(0.378 \times q + 0.622)}$$

Where q represents specific humidity, unit: kg/kg; E is the actual vapor pressure in the air in unit hPa; p is the surface pressure in unit hPa. For saturated vapor pressure E_S, it can not only affect the deposition rate of atmospheric nitrogen, but its loss also significantly restricts the water use efficiency of some trees (Lei et al., 2017), therefore it is important to estimate it with as low error as possible. Most of the current articles draw on the estimation method published by Bolton (1980). This method has been widely cited due to its high accuracy from − 30℃ to 35℃ and simple calculation process (Ding et al., 2021; Hardwick et al., 2015).

$$E_S = 6.112 \times e^{\left(\frac{17.67 \times t}{t+243.5}\right)}$$

Where t is temperature in °C.

2.2.3. Trend analysis

Combining Mann–Kendall (MK) test and Theil–Sen median trend, this study analyzed the temporal and spatial characteristics of GPP and various factors from 1997 to 2017. The MK test is a nonparametric test method (Hamed and Ramachandra Rao, 1998; Hamed and Rao, 2008; Libiseller and Grimvall, 2002). It is advantageous because it does not require data to follow a specific distribution and is not affected by a few outliers. It often is combined with Theil–Sen slope estimation to detect the changing trend of long-term series data. The calculation formula is as follows:

$$\alpha = \frac{n\sum_{i=1}^{n}(i \times R_i) - \sum_{i=1}^{n} i \times \sum_{i=1}^{n} R_i}{n \times \sum_{i=1}^{n} i^2 - \left(\sum_{i=1}^{n} i\right)^2}$$

where n is the research period, i represents the year number, and R_i is the value of the independent variable corresponding to the i–th year. α is a linear trend value, >0 represents an increasing trend, otherwise it represents a decreasing trend.

Define the Z statistic as:

$$Z = \begin{cases} \frac{S-1}{\sqrt{Var(S)}}, S > 0 \\ 0\ , \qquad S = 0 \\ \frac{S+1}{\sqrt{Var(S)}}, S < 0 \end{cases}$$

among them:

$$S = \sum_{j=1}^{n-1} \sum_{i=j+1}^{n} sign(R_j - R_i)$$

The sign function formula:

$$sign(R_j - R_i) = \begin{cases} 1, R_j - R_i > 0 \\ 0, R_j - R_i = 0 \\ -1, R_j - R_i < 0 \end{cases}$$

Var variance calculation formula:

$$Var(S) = \frac{n(n-1)(2n+5)}{18}$$

where sign is a sign function, this paper judges the significance of the change trend of the R factor at the significance level p = 0.05.

2.2.4. Partial correlation analysis

Partial correlation analysis is called net correlation analysis, which is used to analyze the linear correlation between two variables under the condition of controlling the linear influence of other variables. When the number of control variables is one, the partial correlation coefficient is called the first-order partial correlation coefficient. When the number of control variables is two, the partial correlation coefficient is called the second-order correlation coefficient. We used the method of Huang et al. (2020) to determine the significance of each partial correlation, adjusted the p-value, determined the partial correlation information between the two factors on the pixel, and then used R to output the partial correlation layer. We performed all analyses on a global scale. The partial correlation coefficient between GPP and its influence factors was calculated according to the following formula:

$$R_{xy} = \frac{\sum_{i=1}^{n}\left[(x_i - \bar{x}_-)(y_i - \bar{y}_-)\right]}{\sqrt{\sum_{i=1}^{n}(x_i - \bar{x}_-)^2 \sum_{i=1}^{n}(y_i - \bar{y}_-)^2}} \quad (10)$$

where r_{xy} is the correlation coefficient between variables x and y; x_i is the factor of the i–th year (SM, PRE, TEM, ND, CO_2); y_i is the average GPP in the i–th year; x is the average value of each factor during the study period; y is the average annual GPP during the study period.

This study has 6 variables: GPP, SD, PRE, TEM, ND, CO_2, the formula of the fourth–order sample partial correlation coefficient of any two variables GPP and SD is:

$$R_{GPP \cdot SD\_PRE \cdot TEM \cdot ND \cdot CO_2} = \frac{R_{GPP \cdot SD \cdot PRE \cdot TEM \cdot ND} - R_{GPP \cdot CO_2\_PRE \cdot TEM \cdot ND} R_{SD \cdot CO_2 \cdot PRE \cdot TEM \cdot ND}}{\sqrt{(1 - R^2_{GPP \cdot CO_2\_PRE \cdot TEM \cdot ND})(1 - R^2_{SD \cdot CO_2 \cdot PRE \cdot TEM \cdot ND})}} \quad (11)$$

where $R_{GPP.SD\_PRE.TEM.ND.CO2}$ represents the partial correlation coefficient between GPP and SD after removing the influence of the variables PRE, TEM, ND, and CO_2; $R_{GPP.CO2\_PRE.TEM.ND}$ and $R_{SD.CO2\_PRE.TEM.ND}$

represent respectively the correlation between GPP and CO_2, SD and CO_2 after removing the influence of PRE, TEM and ND. In addition, t–test is used to determine the significance of the correlation between the two variables, and if $p < 0.05$, the 95% confidence significance test is passed, otherwise, it is not significant.

2.2.5. Assess the relative contribution of soil drying and climate factors to GPP

To analyze the relative contribution of SD, climate factors, and residual factors to GPP changes, we used the linear regression analysis (Liu et al., 2019b) to calculate the actual GPP trend. Taking the corresponding GPP trend data as the dependent variable and each factor datum as the independent variable, the following equation is constructed:

$$\begin{aligned}\frac{d_{GPP}}{dt} &= \frac{d_{SD}}{dt}\cdot\frac{\partial_{GPP}}{\partial_{SD}} + \frac{d_{PRE}}{dt}\cdot\frac{\partial_{GPP}}{\partial_{PRE}} + \frac{d_{TEM}}{dt}\cdot\frac{\partial_{GPP}}{\partial_{TEM}} + \frac{d_{ND}}{dt}\cdot\frac{\partial_{GPP}}{\partial_{ND}} + \frac{d_{CO_2}}{dt}\cdot\frac{\partial_{GPP}}{\partial_{CO_2}} + \varepsilon \\ &= \mathrm{Con\_}SD + Con\_PRE + Con\_TEM + Con\_ND + Con\_CO_2 + Con\_\varepsilon \\ &= \mathrm{Con\_}SD + Con\_Clim\cdot + Con\_\varepsilon\end{aligned}$$

where $\frac{d_{GPP}}{dt}$ represents the Theil–Sen median trend of GPP changes, $\frac{\partial_{GPP}}{\partial_{SD}}$, $\frac{\partial_{GPP}}{\partial_{PRE}}$, $\frac{\partial_{GPP}}{\partial_{TEM}}$, $\frac{\partial_{GPP}}{\partial_{ND}}$, $\frac{\partial_{GPP}}{\partial_{CO_2}}$ represent the partial derivative values between GPP and SD, PRE, TEM, ND, and CO_2 respectively. From the definition of the formula, each partial derivative eliminates the influence of the other two variables, and is equal to the corresponding second-order partial correlation coefficient (see method 2.24 for details), Con_SD, Con_PRE, Con_TEM, Con_ND and Con_CO_2 represent the contribution value of each factor to GPP, Con_Clim is the total contribution of climate factors (PRE, TEM, ND, CO_2), Con_ε represents the contribution of the residual factors (other factors not considered). The study mainly uses free code R to calculate the relative importance of SD and climate factors to changes in terrestrial GPP, and obtains the relative contribution of different factors to changes in GPP.

2.2.6. Soil drying and climate factors offset analysis

To further clarify the contribution of SD to offset climate factors to GPP changes, we calculated the proportions of net GPP offset (NGOP), that is, SD (negative contribution) offset climate factors (positive contribution) to GPP changes. The calculation formula is as follows:

$$S_{NGOP} = \left|S_{SD_{decreasing}}\right| \div \left|S_{CF_{increasing}}\right| \times 100\%$$

$$S_{SD_{decreasing}} = \left|S_{SD} - S_{SD_{increasing}}\right|$$

$$S_{CF_{increasing}} = \left|S_{CF} - S_{CF_{decreasing}}\right|$$

where S_{NGOP} is the proportion of SD offsetting the contribution of climate factors to GPP changes. $S_{SDdecreasing}$ is the negative contribution zone of SD to GPP changes, $S_{CFincreasing}$ is the zone where climate factors contributes positively to GPP, S_{SD} is the zone where SD contributes to GPP, $S_{SDincreasing}$ is the positive contribution zone of SD to GPP, S_{CF} is the climate factor's contribution zone to GPP, $S_{CFdecreasing}$ is the climate factor's negative contribution zone to GPP.

2.2.7. Soil drying and climate factors contribute to the main control zone

On the pixel scale, we summarized the calculated contribution rates of SD, climate factors, and residual factors and individually mapped the contribution rates of these three factors to the three different RGB grid bands. We determined the depth of each band color by the contribution value of various factors, that is, the darker the color, the higher the contribution rate of the factor. Finally, we merged the three bands into a raster layer. The color displayed on the raster layer was the pixel scale of the contribution distribution of the different types of factors. This calculation was carried out by free code R for RGB analysis, and finally, we obtained the main control area of different factors to GPP changes, and the technical flow chart of this paper as shown in Fig. 1 (Fig. 1).

3. Results

3.1. GPP changes

From 1997 to 2017, the global GPP averaged 834.74 g C m^{-2} yr^{-1}. GPP followed a trend of gradually decreasing from near the equator to the north–south latitude. The high-value zones were located mainly in South America, central Africa, and Southeast Asia, with an average value exceeding 2700 g C m^{-2} yr^{-1}. The low-value zones were distributed mainly in the high-latitude zones, including the American West, western China, Australia, South Africa, northern Russia, and western South America. The average value was <300 g C m^{-2} yr^{-1} (Fig. S1). In terms of continents, South America had the largest GPP, which was 2.4 times higher than the global average. We observed that tropical, warm temperate, and cold temperate zones accounted for 44%, 32%, and 15% of global GPP, respectively (Fig. S1), and observed lower values in arid and polar climate zones. In addition, the global annual value of GPP fluctuated over time (Fig. S2); the highest value (861.41 g C m^{-2} yr^{-1}) appeared in 2000, and the lowest value (821.4 g C m^{-2} yr^{-1}) appeared in 2018.

According to the MK test, the GPP mutation occurred in 2001 (Fig. 2a). It increased at a rate of 8.99 per year before 2001 and decreased at a rate of 0.3 per year after 2001. Overall, for 21 years, the global GPP has declined at a rate of 0.68 per year (Fig. 2b). Similarly, the same result was obtained in the study of Williams et al. (2014) and this result may have been affected by high temperatures and drought. In addition, GPP was significantly different in climatic zones, with the highest percentage of GPP declining in the tropical zone (71%, 46% significantly reduced), and the highest percentage of GPP increasing in the polar zone (54%, 19% significantly increased; Fig. 2c, d). The confidence level of the MK test was 0.05, and the GPP trend values were divided into five levels according to the standard (Table S1, Fig. 2e). We found that 39% of the study area GPP showed a downward trend, which was distributed mainly in high-latitude areas, near the equator (such as southern South America, Central Africa, Central Asia), which accounted for about 16% of the study area. The GPP declined significantly and was distributed mainly in South America North, central Africa, southern Russia, southern North America, and northern India. At the same time, 12.9% of the study area had a significant increase in GPP, which occurred mainly in China, India, northern Europe, eastern Asia, and eastern Southeast Asia (Fig. 2e).

To understand the temporal and spatial changes of global GPP, we used the moving window analysis to evaluate the trend value of GPP. A moving window every 7 years was the research period ($P < 0.05$). We found that the spatial change trend of GPP presented a large time difference (Fig. S2), which was consistent with the MK test analysis (Fig. 2c). By comparing the rate of change in GPP in every 7 years (Fig. S3a), we found that the rate of evolution of GPP decreased slightly, but the change was gentle. In addition, combined with the mean slope and spatial variation of GPP sliding (Fig. S3b, Fig. S2), we found that the rate of decrease was the fastest from 2000 to 2006, and occurred mainly in South America, South China, Oceania, and parts of Africa. From 2011 to 2017, GPP increased the fastest, and occurred mainly in China, the United States, and parts of South America. This finding indicated that China's vegetation grew rapidly during this period, which was consistent with the conclusion of Chen et al. (2019a). Through the use of moving window analysis, we found that, especially after 2011, fundamental changes had taken place, and GPP was on the rise.

3.2. Effect of soil drying on GPP

In general, from 1997 to 2017, SM decreased at an average annual rate of 0.16×10^{-3} km^2. More than half of the area was drying out and was distributed mainly in Europe, the United States, Brazil, Central

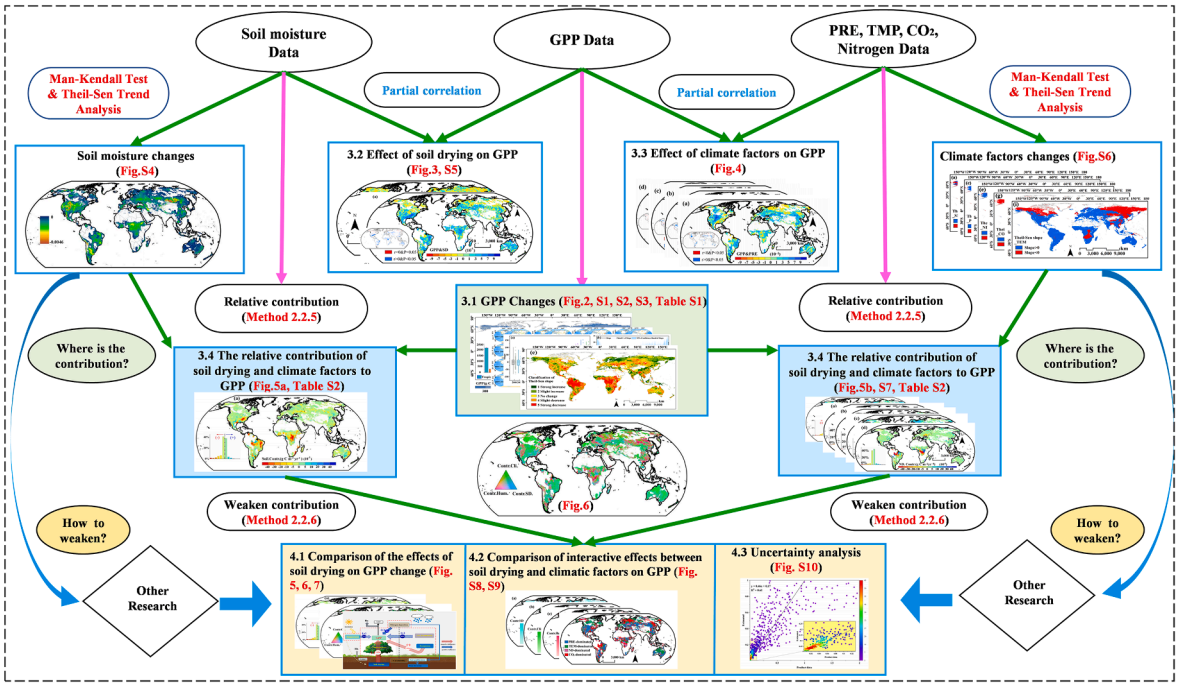

Fig. 1. Technical flow chart.

Africa and surrounding areas, southern China, and Australia (Fig. S4). As the SM changed, GPP also gradually changed. Based on the partial correlation method, 61% of SM and GPP were positively correlated, and 39% were negatively correlated (Fig. S5). In Oceania and Africa, this correlation was even higher. In addition, in the arid zone and the warm temperate zone, GPP and soil water changes were similar.

It is understood that the greening of vegetation in many regions of the world leads to SD (Deng et al., 2020a). The SD area accounts for a large proportion of the global surface (64.7%), and the influence on terrestrial GPP is gradually strengthening. Specifically, the annual decrease of 0.12 g C m^{-2} yr^{-1} in GPP is related to SD. In SD areas in particular, more than half (63.7%) of the area GPP and SM changes were synchronized (12% significant) (Fig. 3), which were located mainly in the United States, Brazil, Central Africa, Australia, the western edge of Russia, and Southwest China (Fig. 3). In addition, from 1997 to 2017, global GPP and SD showed a significant positive correlation (R = 0.11), especially in warm temperate and tropical zones (Fig. 3b). For the polar zone, however, SD and GPP were significantly negatively correlated (R = − 0.07; Fig. 3b).

3.3. Effect of climate factors on GPP

Among the climate factors, we considered PRE, TEM, CO_2, and ND. We analyzed the correlation between each factor and GPP based on partial correlation. We found that 64% of PRE had a positive correlation with GPP (15% significant; $P < 0.05$), and it was distributed mainly in the central part of North America, the southern part of South America, the southern edge of Russia, and northern China (Fig. 4a). >60% of TEM had a positive correlation with GPP (14% significant), and was distributed mainly near 60 degreesN latitude, northern Canada, Australia, and other regions (Fig. 4b). CO_2 concentration was an important driving factor of GPP (Xu et al., 2019), and we found a positive correlation (16% significant) between 61% of CO_2 regions and GPP (Fig. 4c), which was distributed mainly in northern Canada, Australia, and other regions. In addition, 53% of ND had positive correlation with GPP (4% significant) (Fig. 4e, f).

From 1997 to 2017, the global GPP had a significant positive correlation with the average PRE (R = 0.12, $P < 0.05$). In tropical and arid zones, the correlation was more obvious (R = 0.3, $P < 0.05$; Fig. 4e); however, for polar zones and cold temperate zones, GPP was significantly positively correlated with TEM (R = 0.34; Fig. 4e). By observing the significant changes in GPP and the four climate factors (Fig. 4f), we found that the most significant changes in GPP and PRE were in the cold temperate zone, whereas the most significant changes in GPP and TEM were in the tropics zone (Fig. 4a). From the perspective of four factors (Fig. 4f), ND played an important role in GPP changes on a global scale (60%), and in tropical (70%), arid (58%), cold temperate (52%), and polar zones (58%). In the warm temperate zone, the changes in GPP and CO_2 were the most significant.

3.4. The relative contribution of soil drying and climate factors to GPP

The SD-induced decrease in GPP offset 35% of the climate factors–-driven increase area over the same period (Fig. 5c). The weakened zones were distributed mainly in the northeastern United States, central Brazil, central and southern Africa, Australia, northern and southern Russia, and southwestern China. Separating the two main factors, SD contributed negatively to GPP (−0.25 g C m^{-2} yr^{-1}, about 19%; Table S2, Fig. 5a). In terms of climate zones, the most contributory region were tropical (−85%) and warm temperate zones (−41.5%). At the continent level, the largest contribution was Africa (−85%), which was concentrated in Swaziland, Kenya, Mozambique, Malawi, and other southeastern African countries. Followed by South America (−65%), mainly in Brazil, Venezuela, and Argentina. In addition, GPP was deeply affected by SD in places such as San Marino in southern Europe, Solomon Islands in Australia, and Malaysia in Southeast Asia.

Climate factors (PRE, TEM, CO_2, ND) had a positive contribution with GPP changes (0.54 g C m^{-2} yr^{-1}, about 33%; Fig. 5b). In the SD zone, each factor showed obvious spatial heterogeneity (Fig. S7). In general, CO_2 had the greatest positive contribution to GPP change (24%); TEM and PRE contributed 22% and − 21%, respectively; and ND contributed the least (8%) (Table S2). Among them, PRE had the largest negative contribution in central South America, whereas it was mainly positive in the United States and China. TEM had the largest positive contribution in central South America, while it was mainly negative in central Africa. ND mainly had a positive contribution in Central South

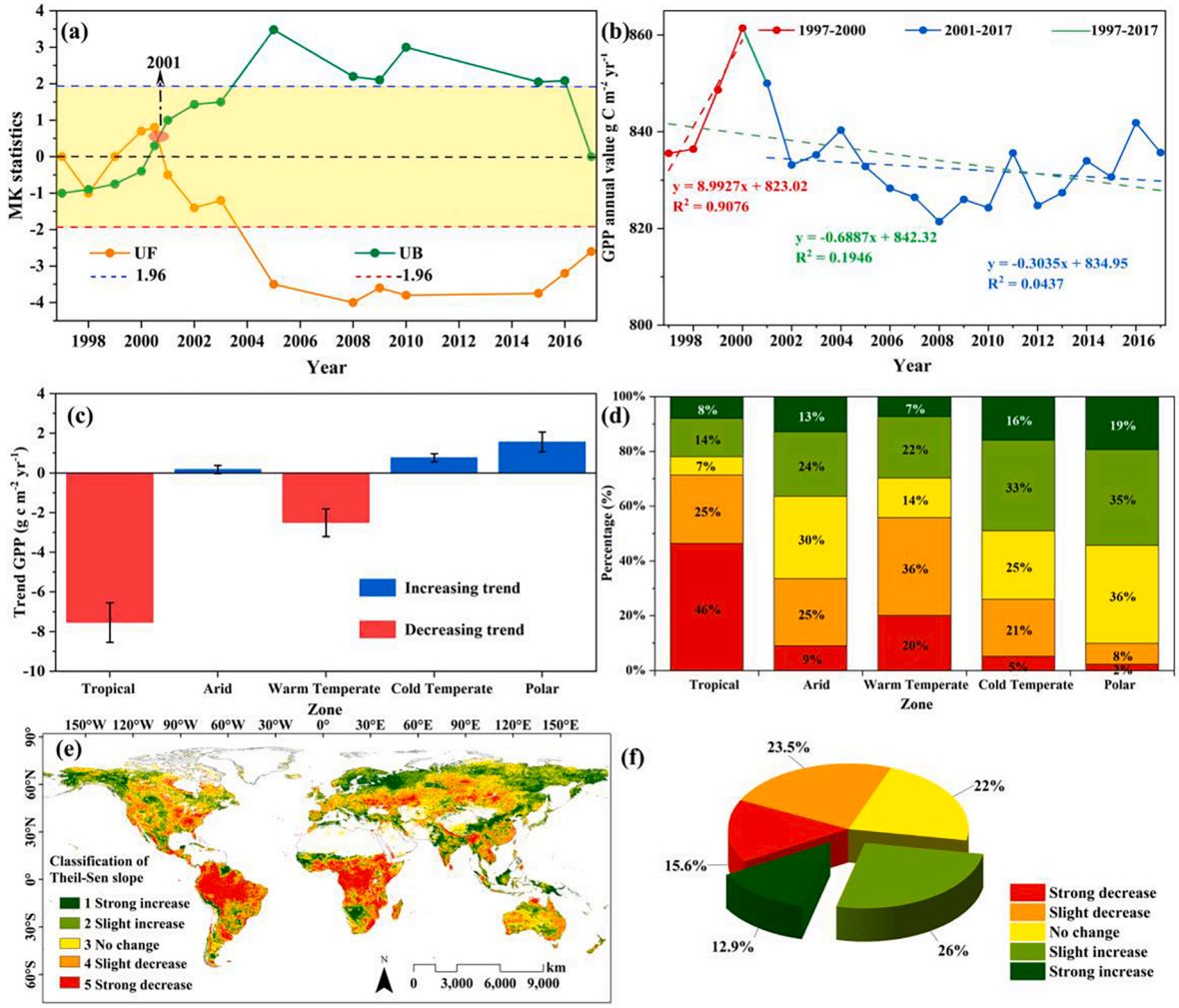

Fig. 2. Trend characteristics of GPP on the global pixel scale from 1997 to 2017. Fig. 2a-b shows the MK test and linear trend of the global average GPP anomaly; the red, green, and blue lines in Fig. 2b are the regression equations for 1997–2000, 1997–2017, and 2001–2017, respectively; Fig. 2c is The distribution of the Theil-Sen's slope climate zone; Fig. 2e represents the significant change of GPP, Fig. 2d is the proportion of each category of climate in Fig. 2e, and Fig. 2f is the area statistics of the significant changes in Fig. 2e. (For interpretation of the references to color in this figure legend, the reader is referred to the web version of this article.)

America and Central Africa. CO_2 exceeded 70% area and had a positive contribution. Similarly, Qiu et al. (2020) demonstrated that CO_2 concentration was a key factor in the relationship between sun-induced chlorophyll fluorescence and GPP. In general, climate factors had a large positive contribution in central South America, China, and northern Europe, whereas it had a negative contribution in central Africa and elsewhere the contribution was small.

According to the triangular image RGB method, we obtained the dominance of three factors on GPP changes. Fig. 6 shows the control distribution of SD, climate factors, and residual factors (i.e., all other factors that cannot be explained by climate factors and SD, such as extreme drought, ecological engineering) on GPP changes from 1997 to 2017. We found that climate factors explained 37% of global GPP changes (Fig. 6; Fig. S8); in contrast, SD explained 18% of these changes (Fig. 6; Fig. S8). Note that the residual factors dominated most regions, explaining 45% of the GPP change. For example, in southern Russia, southern China, Turkey, central Africa, and the United States, it played a vital role in terrestrial GPP (Fig. 6; Fig. S8), which may be related to ecological engineering related to human activities (Fig. S7). For example, China's human engineering has played a certain role in the increase of GPP, especially in the Three North Shelterbelt area (Peng et al., 2012). Additionally, the changes in GPP in areas dominated by the residual factors also may be attributed to the effects of extreme droughts, such as in central Africa and northern Canada (Schwalm et al., 2017). Note that in areas where residual factors dominated, SD still offset the positive impact of climate factors (Fig. 5c, Fig. 6).

4. Discussion

4.1. Comparison of the effects of soil drying on GPP change

In this study, we found that SM had a negative contribution to the overall growth of GPP (19%) (Fig. 7). This effect was closer to the results of previous studies (Stocker et al., 2019) and had a negative contribution to SM. About 66.3% of the areas in the region were decreasing in SM. This may have been due to the fact that SD has exacerbated the stress effect of drought and weakened the water use efficiency of vegetation (Green et al., 2019), thereby affecting the vegetation's normal growth.

Taking South America as an example, we found that in the past 21 years, the GPP in this region (especially in Brazil, Argentina, and Venezuela) has continued to decrease (Fig. 2e), and this may be related to a reduction in soil water (Fig. 6, Fig. S6). This phenomenon was also found in the research of He et al. (2021). The drought in Brazil and other places has increased, leading to a sharp decline in vegetation productivity. In addition, the results on the pixel scale also supported these conclusions (Fig. 5a). Taking tropical regions as an example, we found a

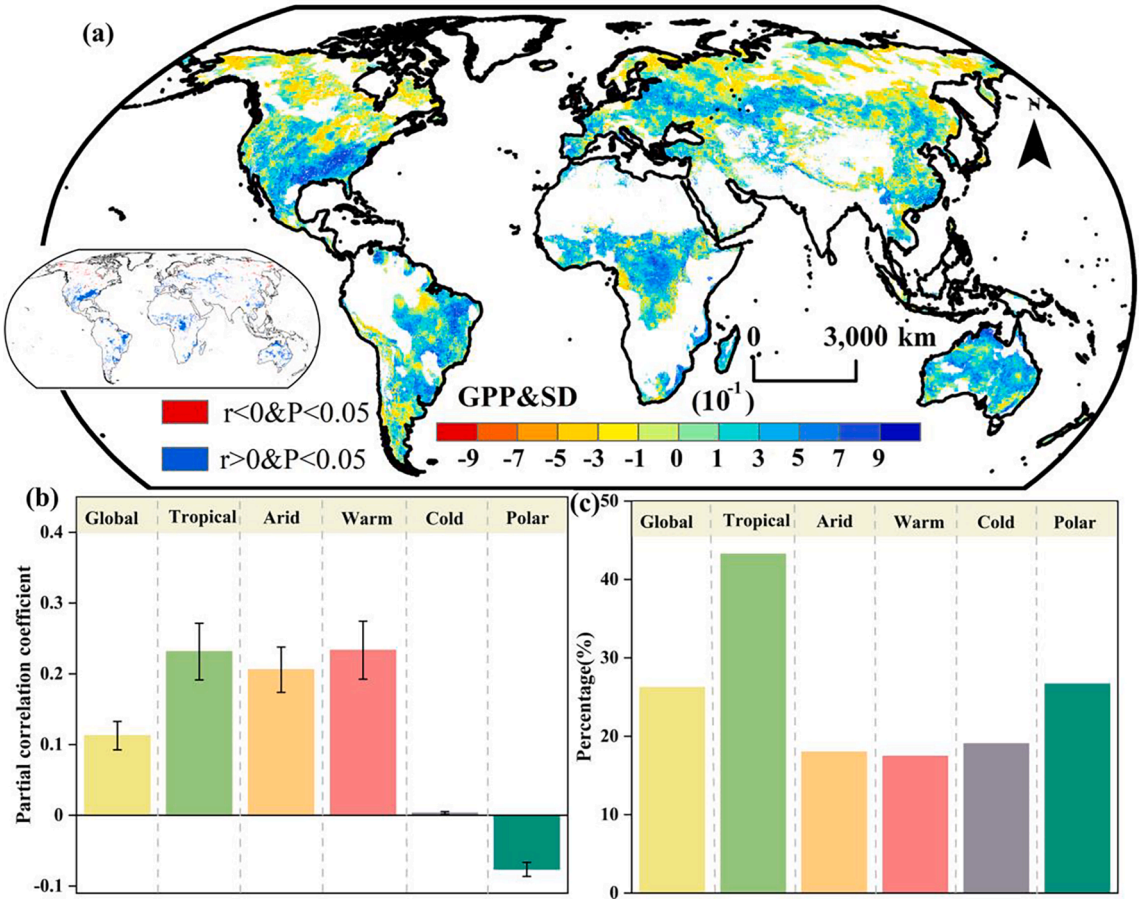

Fig. 3. The spatial correlation pattern of GPP and soil drying from 1997 to 2017. (a) Represents the partial correlation distribution map of GPP and soil drying, where the small graph represents the comparative correlation coefficient ($r > 0, r < 0$) and its relative significance level, where blue and red are significantly positive and negative respectively related area; (b) represents the partial correlation coefficient of (a) in each climatic zone; (c) The spatial distribution ratio of significant changes between GPP and soil drying, that is, the percentage of areas where soil drying and GPP change significantly at the same time to the areas where GPP has significant interannual changes. (For interpretation of the references to color in this figure legend, the reader is referred to the web version of this article.)

significant positive correlation between SD and GPP reduction (R = 0.2, and GPP both accounted for a significant area of 43%). When the SM in the region dropped significantly, GPP also decreased. This phenomenon coincided with the research results of Liu et al.—that is, SD was one of the dominant factors restricting photosynthesis in tropical regions (Liu et al., 2015). In the cold temperate arid area of high latitudes (e.g., Xinjiang, Tibet, and other places in China), we found that the SM and GPP decreased at the same time. This phenomenon was consistent with the previous observations made by Yuan et al. that SD in this area greatly reduced the carbon absorption efficiency of terrestrial ecosystems (Yuan et al., 2016).

Intensified SD not only substantially changed the landscape of the soil, but also changed the biogeochemical cycle and the photosynthetic productivity of the terrestrial ecosystem. In our research, we found that SD in most parts of the world caused a large decline in vegetation productivity. For this reason, we suggest that management measures, such as changing the planting date and establishing a new irrigation system, be used to increase the effect of vegetation carbon accumulation, which can greatly reduce the carbon loss caused by the drying of soil water (Tang et al., 2018; Tian et al., 2019).

4.2. Comparison of interactive effects between soil drying and climatic factors on GPP

In central and northern South America, central Africa, and southern North America, the decline in GPP was spatially consistent with the decline in SD, PRE, and ND. This result was consistent with the findings of Madani et al. (2020) and Chen et al. (2017). The ubiquitous positive partial correlation between GPP and the three variables (SD, PRE, and ND) also supported this finding (Fig. 2e, Fig. 3b, Fig. 4e, Fig. S6). The simultaneous reduction of PRE and ND under the background of continuous soil water drying caused a reduction in terrestrial GPP (Yao et al., 2020; Lee et al., 2018).

The decline of GPP in some regions was significantly positively correlated with the interannual changes of PRE, TEM, and SD, such as in the United States and Australia (Fig. 2e, Fig. S6). Nevertheless, PRE and TEM in these two regions generally increased, and SM decreased (Fig. 2e, Fig. S6), which may have been related to the decrease of GPP yield in this region because of heat stress caused by drought. This result was consistent with Pickering et al.'s discovery of reduced SM and litter loss in the United States and Australia (Pickering et al., 2010). At the same time, this result showed that the reduction of soil water content had an important negative impact on the yield of GPP (Stocker et al., 2018). According to the research of Dodd et al. (2015), SD in the future may aggravate the decline of GPP in these two regions (Dodd et al., 2015). In addition, there has been a decrease in PRE and an increase in SM in southern Australia, but the GPP in the region is still following a downward trend (Fig. 3e, Fig. S6). Zscheischler et al. (2014) also obtained the same conclusion, but believed that this trend may be caused by the influence of extreme high temperature on vegetation activities and legacy effects. At the same time, the interference of human activities, such as the deforestation of forests and woodlands as well as agricultural expansion, may be leading reasons for the decline in vegetation coverage in Australia (Donohue et al., 2010; Doughty et al.,

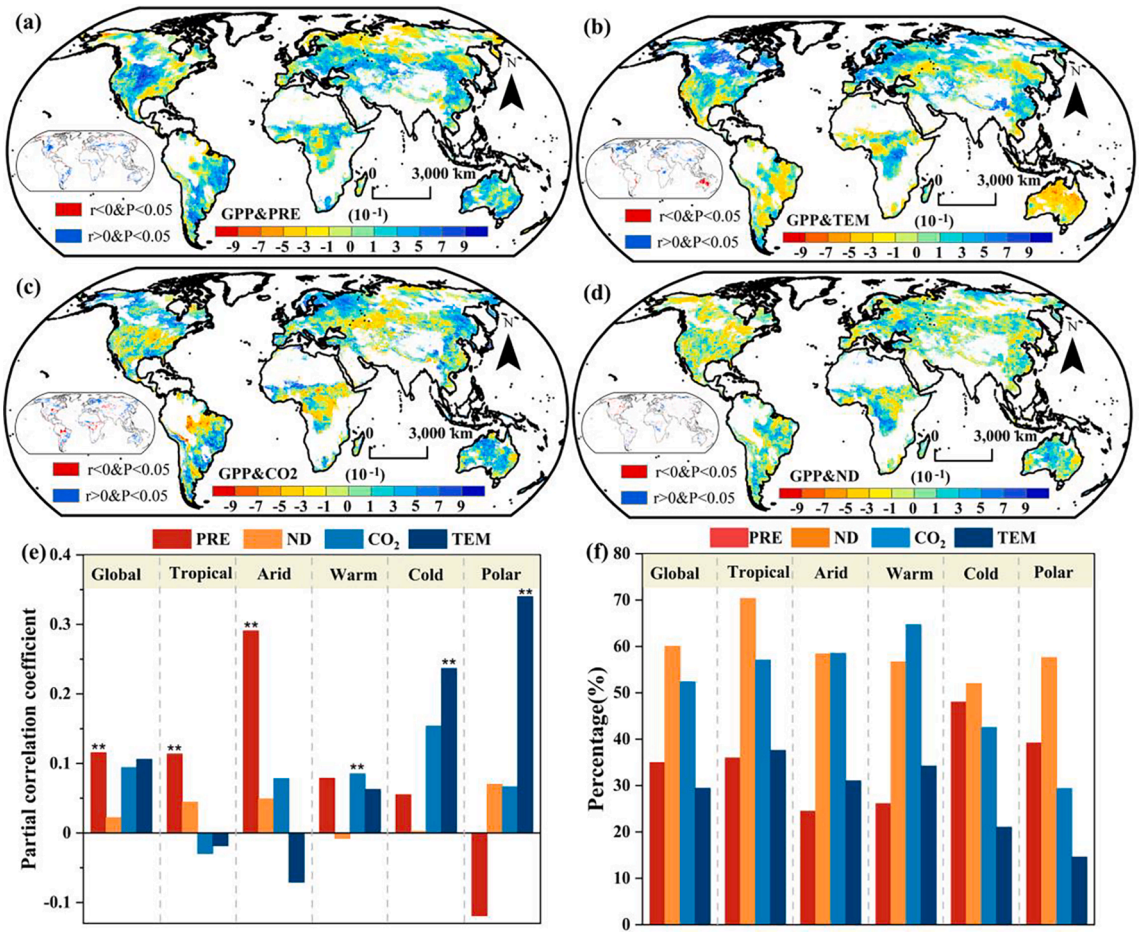

Fig. 4. The correlation between GPP and climate factors from 1997 to 2017. The spatial partial correlation pattern of GPP and PRE (a), TEM (b), CO_2 (c), and ND (d). And the partial correlation coefficient (e) on the climate zone, and the proportion of GPP and each factor are significant areas. The small graphs in (a), (b), (c), (d) represent the concentration of PRE, TEM, CO_2, the correlation coefficient of ND and GPP ($r > 0, r < 0$) and its relative significance level ($P < 0.05$, $P > 0.05$). (e) the partial correlation coefficients of the global annual average GPP and the four driving factors on the climate zone, the driving factors are respectively annual average PRE, TEM, CO_2, and annual average ND. (f) the proportion of GPP and climate factors simultaneously significant. That is, the areas where each climate factors factor and GPP change significantly at the same time account for the percentage of the areas where GPP interannual changes are significant.

2018).

The reduction of GPP is widely distributed in climate-controlled regions (Humphrey et al., 2018), including central Canada, northern United States, central Africa, South Africa, western and northern Europe, central and southern South America, western and central Russia, Kazakhstan, northern Australia, and the plateau region of northern China (Fig. 6). Most of these zones match those with decreasing CO_2 concentration (Fig. 6, Fig. S6), which agreed well with the findings of Schwalm et al. (2020) that CO_2 concentration was the main factor affecting GPP changes. According to his analysis of the main factors of GPP, the continuous rise of atmospheric CO_2 occupied the first place, and 58% of vegetation was affected mainly by CO_2 (Schwalm et al., 2020). In addition, we found that SD generally has increased in some of these regions (i.e., plateau areas in northern China, western and northern Europe, western Russia, Kazakhstan, East and South Africa, and eastern Brazil) (Fig. S6a, b). This result confirmed the relevant research conclusions of Deng et al. that the continuous growth of vegetation and photosynthetic effects require adequate water supply, and the pressure of water consumption by human production and life and other ways has gradually become prominent (Deng et al., 2020b). Most important, the partial correlation between GPP and SD (or PRE or ND or TEM; Fig. 3a, Fig. 4a, b, c, d) showed that the decline in SM and climate fluctuations together determined the amount of available water and the yield of photosynthesis for vegetation. This result was consistent with the findings of Van et al. that the SM had a strong regional influence on GPP, but the differences between different climatic regions were very large (Van et al., 2018). We found that this phenomenon was particularly obvious in tropical regions (Fig. 3c, Fig. 4e), which explained the decline in GPP in the region (Fig. 2e). Changes in GPP may be affected mainly by extreme drought (Schwalm et al., 2012; Poulter et al., 2014; Flack-Prain et al., 2019; Xu et al., 2019; Fang et al., 2019). We found that in Africa (especially the Democratic Republic of the Congo) and Europe (Ukraine), ND was the main reason for the changes in GPP (Fig. 6, Fig. S9). The GPP of these two regions decreased as the ND decreased, which was the same result as the conclusion of Schwalm et al. (2020). Nitrogen is an essential element for plant growth, and an increase in ND usually promoted plant growth (Templer et al., 2012). In Africa (especially Gabon, Central Africa), Asia (Russia), and Southeast Asia, the main cause of the changes in GPP is CO_2 (Fig. 6, Fig. S9). We found that the CO_2 concentration in Africa and Asia was continuously decreasing, whereas it is continuously increasing in Southeast Asia. Therefore, improving the conditions of CO_2 concentration will increase vegetation photosynthesis. These findings confirmed the conclusion of Vuichard et al. (2019). In addition, studies have shown that primary productivity and carbon storage are limited by the availability of terrestrial nutrients (Wieder et al., 2015), that is, when the content of climatic factors is lower than the optimal line for photosynthesis, or higher than, the photosynthetic rate of the leaves will decrease because of insufficient or excessive nutrients (Medlyn et al., 2015; Liu et al., 2018; Vuichard et al., 2019; Wang et al., 2020b). Therefore, proper nutrient conditions are

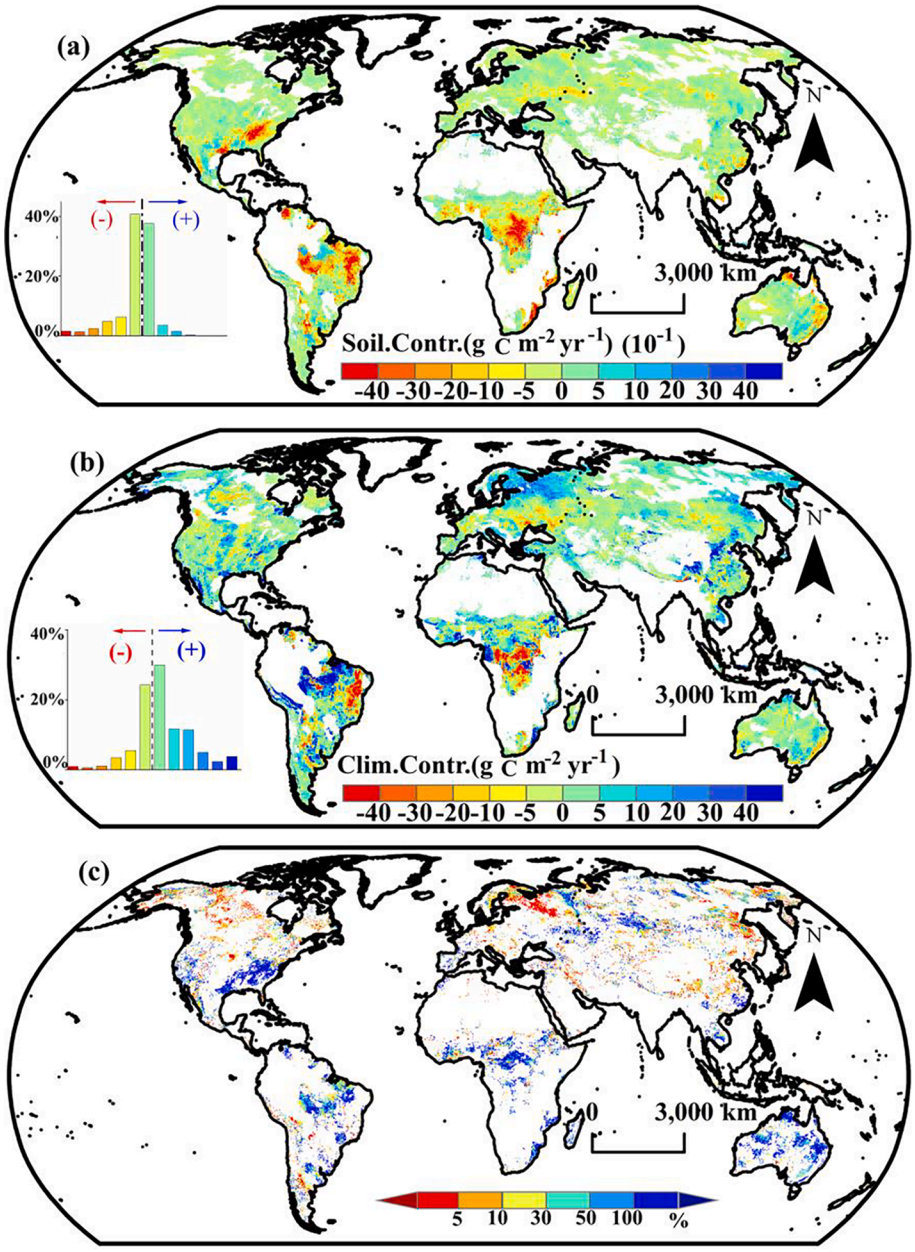

Fig. 5. The spatial contribution of soil drying (a) and climate factors (b) to terrestrial GPP changes from 1997 to 2017, and the percentage difference between the contribution of climate factors and soil drying (c).

conducive to the occurrence of photosynthesis.

4.3. Uncertainty analysis

This study evaluated the impact of SD and climate factors on terrestrial primary productivity and promoted a deeper understanding of vegetation carbon driving mechanisms. Our research, however, had some limitations and uncertainties. First, in terms of the GPP remote sensing data, we did not select more remote sensing data for comparative analysis. This uncertainty affected the comprehensive understanding of changes in vegetation productivity to a certain extent. In addition, the simulation accuracy of ND also has certain shortcomings (Fig. S10). Second, in terms of content, due to the limitations of data and methods, the dynamic changes of the contributions of various factors to GPP have not been considered, which may be an aspect that should be paid attention to in the future. In addition, because our research is mainly about the response of plant primary productivity and SM and climate factors, we did not quantitatively analyze the impact of human activities and extreme climatic conditions. Although we considered factors that effect GPP changes in many aspects, we found that residual factors (human activities and extreme drought) still accounted for a large proportion of GPP changes. Therefore, in this study, we used residual factors to represent other unconsidered factors, in fact, when analyzing the reasons for the changes in GPP, we considered and retained the impact of other factors on GPP. Because of the limitation of data and workload, this study did not provide detailed management measures for vegetation productivity in different regions. In view of these uncertainties and limitations, the next step of research should promote the dynamic calculation of the vegetation-driving mechanism as one of the important tasks. This research should be conducted as soon as possible to provide a richer understanding of vegetation carbon accumulation on a global scale.

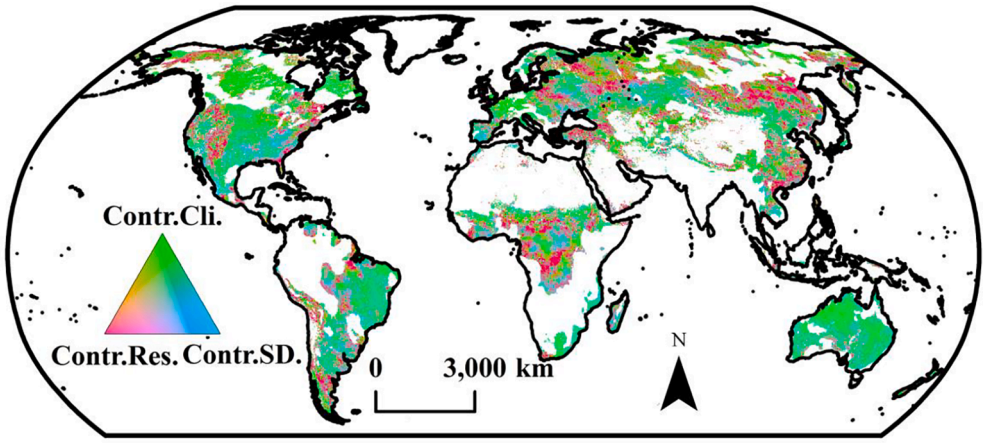

Fig. 6. The dominant area of climate factors, soil drying and residual factors (ecological engineering, extreme drought) on GPP changes from 1997 to 2017. The figure depicts the dominant contribution zones of climate factors, soil drying and residual factors to GPP changes. By conducting two separate experiments of climate factors drive and soil drying drive first, in addition, a residual factor driving analysis was carried out, the RGB synthesis method is used to divide the image with the relative influence of climate factors, soil drying and residual factors (see method 2.27).

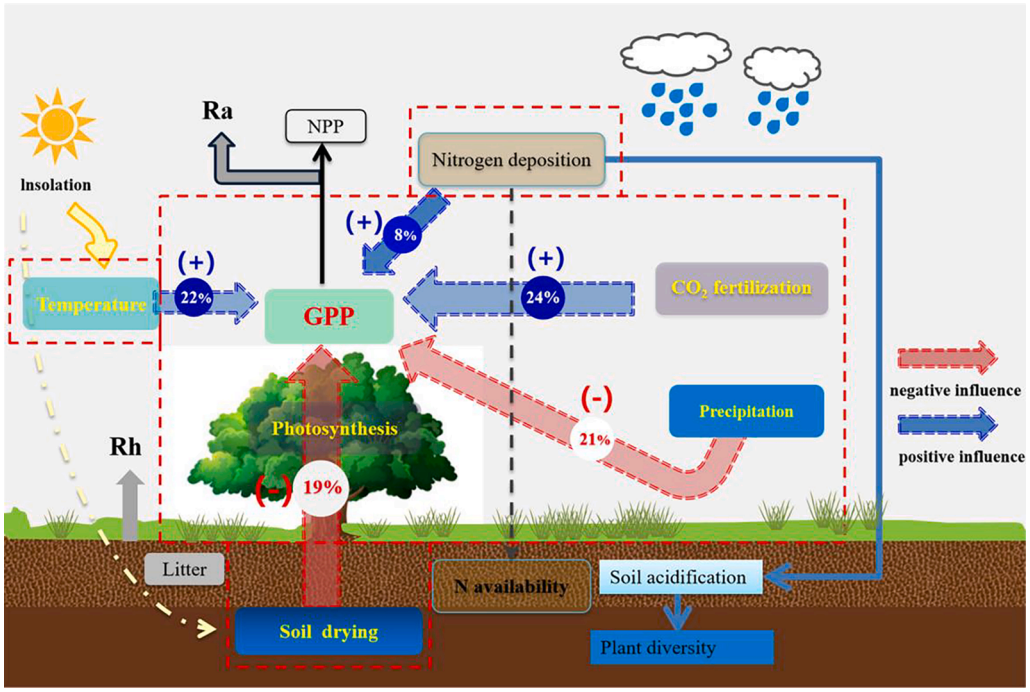

Fig. 7. Schematic diagram of feedback effects of climate factors and terrestrial GPP in soil drying zones. The red dashed box is the main content of this study, the red arrow is a negative effect and the blue arrow is a positive effect. (For interpretation of the references to color in this figure legend, the reader is referred to the web version of this article.)

5. Conclusion

In this study, we used the partial correlation method and linear regression model to quantitatively evaluate the impact of SD and climate factors (PRE, TEM, ND, and CO_2) on terrestrial GPP. We quantified the different ratio of the contribution of SD and climate factors interaction to GPP. Our conclusions follow:

1) From 1997 to 2017, the global GPP showed an insignificant decline, and GPP began to decline in 2001. The rate of change before the mutation of GPP was 30 times that after the mutation. Additionally, 15.6% of GPP decreased significantly, mainly distributed in central and northern South America, Central Africa, Southern Russia, Southern North America, and Northern India.
2) Globally, SD and GPP were positively correlated (63.7%), Specifically, 19% of GPP changes were SD contributions.
3) Climate factors (PRE, TEM, CO_2, ND) all had a positive correlation with GPP. Among them, CO_2 concentration contributed the most to GPP (24%); TEM and PRE contributed 22% and − 21%, respectively; and ND contributed the least (8%), which indicated that CO_2 was the most important driving factor for GPP changes in SD zones.
4) An SD-induced decrease in GPP offset 35% of the climate factors–-driven increase area over the same period, which was distributed primarily in the northeastern United States, central Brazil, central and southern Africa, Australia, northern and southern Russia, and southwestern China.
5) Using the triangular image RGB method, we found that the main control areas of SD, climate factors, and residual factors to GPP change were 18%, 37%, and 45%, respectively.

This study provided further insight into the driving mechanism of terrestrial primary productivity, emphasized that SD plays an increasingly significant role in terrestrial GPP changes, and distinguished and

quantified the contribution of SD and climate factors, which provided a basic data reference for exploring the mechanism of vegetation carbon accumulation under global change.

6. Data Availability Statement

The fundamental data used in our study is available in the public, and their websites are provided in the "2. Materials and methods" section and other data are available from the corresponding author upon reasonable request.

CRediT authorship contribution statement

Huan Chen: Validation, Visualization, Writing – original draft. **Xiaoyong Bai:** Conceptualization. **Yangbing Li:** Conceptualization. **Qin Li:** Formal analysis, Methodology. **Luhua Wu:** Formal analysis, Methodology. **Fei Chen:** Resources, Software, Supervision, Writing – review & editing. **Chaojun Li:** Resources, Software, Supervision, Writing – review & editing. **Yuanhong Deng:** Resources, Software, Supervision, Writing – review & editing. **Huipeng Xi:** Resources, Software, Supervision, Writing – review & editing. **Chen Ran:** Resources, Software, Supervision, Writing – review & editing. **Xuling Luo:** Resources, Software, Supervision, Writing – review & editing. **Min Liu:** Resources, Software, Supervision, Writing – review & editing.

Declaration of Competing Interest

The authors declare that they have no known competing financial interests or personal relationships that could have appeared to influence the work reported in this paper.

Acknowledgements

This research work was supported jointly by the Strategic Priority Research Program of the Chinese Academy of Sciences (No. XDB40000000 & No. XDA23060100), National Natural Science Foundation of China (No.42077455), Western Light Talent Program (Category A) (No. 2018-99), United fund of karst science research center (No. U1612441).

Appendix A. Supplementary data

Supplementary data to this article can be found online at https://doi.org/10.1016/j.ecolind.2021.107953.

References

Anav, A., Friedlingstein, P., Beer, C., Ciais, P., Harper, A., Jones, C., Tortarolo, G.M., Papale, D., Parazoo, N.C., Peylin, P., Piao, S.L., Sitch, S., Viovy, N., Wiltshire, A., Zhao, M.S., 2015. Spatiotemporal patterns of terrestrial gross primary production: a review. Rev. Geophys. 53 (3) https://doi.org/10.1002/2015RG000483.

Arora, V.K., Boer, G.J., Friedlingstein, P., Eby, M., Jones, C.D., Christian, J.R., Bonan, G., Bopp, L., Brovkin, V., Cadule, P., Hajima, T., Ilyina, T., Lindsay, K., Tjiputra, J.F., Wu, T.W., 2013. Carbon concentration and carbon climate feedbacks in CMIP5 Earth System Models. J. Clim. 26, 5289–5314. https://doi.org/10.1175/JCLI-D-12-00494.1.

Ackerman, D.E., Chen, X., Millet, D.B., 2018. Global nitrogen deposition (2°×2.5° grid resolution) simulated with GEOS-Chem. Retrieved from the Data Repository for the University of Minnesota.

Beer, C., Reichstein, M., Tomelleri, E., Ciais, P., Jung, M., Carvalhais, N., Rodenbeck, C., Arain, M.A., Baldocchi, D., Bonan, G.B., Bondeau, A., Cescatti, A., Lasslop, G., Lindroth, A., Lomas, M., Luyssaert, S., Margolis, H., Oleson, K.W., Roupsard, O., Veenendaal, E., Viovy, N., Williams, C., Woodward, F.I., Papale, D., 2010. Terrestrial gross carbon dioxide uptake: Global distribution and covariation with climate. Science 329 (5993), 834–838. https://doi.org/10.1126/science:1184984.

Berg, A., Findell, K., Lintner, B., Giannini, A., Seneviratne, S.I., van den Hurk, B., Lorenz, R., Pitman, A., Hagemann, S., Meier, A., Cheruy, F., Ducharne, A., Malyshev, S., Milly, P.C.D., 2016. Land–atmosphere feedbacks amplify aridity increase over land under global warming. Nat. Clim. Change 6 (9), 869–874. https://doi.org/10.1038/nclimate3029.

Bolton, D., 1980. The computation of equivalent potential temperature. Mon. Weather Rev. 108 (7), 1046–1053. https://doi.org/10.1175/1520-0493(1980)1082.0.CO;2.

Brem, B.T., Gonzalez, F.M., Meyers, S.R., Bond, T.C., Rood, M.J., 2015. Laboratory-measured optical properties of inorganic and organic aerosols at relative humidities up to 95%. Aerosol Sci. Tech. 46 (2), 178–190. https://doi.org/10.1080/02786826.2011.617794.

Cai, W., Cowan, T., Briggs, P., Raupach, M., 2009. Rising temperature depletes soil moisture and exacerbates severe drought conditions across southeast australia. Geophys. Res. Let. 36 (21) https://doi.org/10.1029/2009GL040334.

Castellví, F., Perez, P.J., Villar, J.M., Rosell, J.I., 1996. Analysis of methods for estimating vapor pressure deficits and relative humidity. Agr. Forest Meteorol. 82 (1–4), 29–45. https://doi.org/10.1016/0168-1923(96)02343-X.

Chen, C.C., Park, T., Wang, X.H., Piao, S.L., Xu, B.D., Chaturvedi, R.K., et al., 2019a. China and India lead in greening of the world through land-use management. Nat. Sustain. 2 (2), 122–129. https://doi.org/10.1038/s41893-019-0220-7.

Chen, J.M., Ju, W., Ciais, P., Viovy, N., Liu, R., Liu, Y., Lu, X., 2019b. Vegetation structural change since 1981 significantly enhanced the terrestrial carbon sink. Nat. Commun. 10 (1) https://doi.org/10.1038/s41467-019-12257-8.

Chen, M., Rafique, R., Asrar, G.R., Bond-Lamberty, B., Ciais, P., Zhao, F., Reyer, C.P.O., Ostberg, S., Chang, J., Ito, A., Yang, J., Zeng, N., Kalnay, E., West, T., Leng, G., Francois, L., Munhoven, G., Henrot, A., Tian, H., Pan, S., Nishina, K., Viovy, N., Morfopoulos, C., Betts, R., Schaphoff, S., Steinkamp, J., Hickler, T., 2017. Regional contribution to variability and trends of global gross primary productivity. Environ. Res. Lett. 12 (10), 105005. https://doi.org/10.1088/1748-9326/aa8978.

Ciais, P.h., Reichstein, M., Viovy, N., Granier, A., Ogée, J., Allard, V., Aubinet, M., Buchmann, N., Bernhofer, C., Carrara, A., Chevallier, F., De Noblet, N., Friend, A.D., Friedlingstein, P., Grünwald, T., Heinesch, B., Keronen, P., Knohl, A., Krinner, G., Loustau, D., Manca, G., Matteucci, G., Miglietta, F., Ourcival, J.M., Papale, D., Pilegaard, K., Rambal, S., Seufert, G., Soussana, J.F., Sanz, M.J., Schulze, E.D., Vesala, T., Valentini, R., 2005. Europe-wide reduction in primary productivity caused by the heat and drought in 2003. Nature 437 (7058), 529–533. https://doi.org/10.1038/nature03972.

Crippa, M., Solazzo, E., Huang, G., Guizzardi, D., Koffi, E., Muntean, M., Schieberle, C., Friedrich, R., Janssens-Maenhout, G., 2020. High resolution temporal profiles in the emissions database for global atmospheric research. Sci. Data 7 (1). https://doi.org/10.1038/s41597-020-0462-2.

Deng, Y.H, Wang, S.J., Bai, X.Y., Luo, G.J., Wu, L.H., Chen, F., Wang, J.F., Li, C.J., Yang, Y.J., Hu, Z.Y., Tian, S.Q., Lu, Q., 2020a. Vegetation greening intensified soil drying in some semi-arid and arid areas of the world. Agr. Forest Meteorol. 292-293, 108103. https://doi.org/10.1016/j.agrformet.2020.108103.

Del Grosso, S., Parton, W., Stohlgren, T., Zheng, D., Bachelet, D., Prince, S., Hibbard, K., Olson, R., 2008. Global potential net primary production predicted from vegetation class, precipitation and temperature. Ecology 89 (8), 2117–2126. https://doi.org/10.1890/07-0850.1.

Deng, Y.H., Wang, S.J., Bai, X.Y., Luo, G.J., Wu, L.H., Cao, Y., Li, H.W., Li, C.J., Yang, Y.J., Hu, Z.Y., Tian, S.Q., 2020b. Variation trend of global soil moisture and its cause analysis. Ecol. Indic. 110, 105939. https://doi.org/10.1016/j.ecolind.2019.105939.

Ding, J., Dai, Q., Zhang, Y., Xu, J., Huangfu, Y., Feng, Y., 2021. Air humidity affects secondary aerosol formation in different pathways. Sci. Total Environ. 759, 143540. https://doi.org/10.1016/j.scitotenv.2020.143540.

Dodd, I.C., Jaime, P., Katrin, H., Gabriel, P., Wright, H.R., Blackwell, M., 2015. The importance of soil drying and re-wetting in crop phytohormonal and nutritional responses to deficit irrigation. J. Exp. Bot. 66 (8), 2239–2252. https://doi.org/10.1093/jxb/eru532.

Donohue, R.J., Mcvicar, T.R., Roderick, M.L., 2010. Climate-related trends in australian vegetation cover as inferred from satellite observations, 1981–2006. Global Change Biol. 15 (4), 1025–1039.

Doughty, R., Xiao, X., Wu, X., Zhang, Y., Bajgain, R., Zhou, Y., Qin, Y., Zou, Z., McCarthy, H., Friedman, J., Wagle, P., Basara, J., Steiner, J., 2018. Responses of gross primary production of grasslands and croplands under drought, pluvial, and irrigation conditions during 2010–2016, Oklahoma, USA. Agr. Water Manage. 204, 47–59. https://doi.org/10.1016/j.agwat.2018.04.001.

Fang, W., Huang, S., Huang, Q., Huang, G., Wang, H., Leng, G., Wang, L.u., Li, P., Ma, L., 2019. Bivariate probabilistic quantification of drought impacts on terrestrial vegetation dynamics in mainland china. J. Hydrol. 577, 123980. https://doi.org/10.1016/j.jhydrol.2019.123980.

Flack-Prain, S., Meir, P., Malhi, Y., Smallman, T.L., Williams, M., 2019. The importance of physiological, structural and trait responses to drought stress in driving spatial and temporal variation in GPP across amazon forests. Biogeosciences 16 (22), 4463–4484. https://doi.org/10.5194/bg-16-4463-201910.5194/bg-16-4463-2019-supplement.

GIFFORD, R.M., 1995. Whole plant respiration and photosynthesis of wheat under increased CO_2 concentration and temperature: long-term vs. short-term distinctions for modelling. Global Change Biol. 1 (6), 385–396. https://doi.org/10.1111/j.1365-2486.1995.tb00037.x.

Green, J.K., Seneviratne, S.I., Berg, A.M., Findell, K.L., Stefan, H., Lawrence, D.M., Gentine, P., 2019. Large influence of soil moisture on long-term terrestrial carbon uptake. Nature 565 (7740), 476–479. https://doi.org/10.1038/s41586-018-0848-x.

Hamed, Khaled H., Ramachandra Rao, A., 1998. A modified mann-kendall trend test for autocorrelated data. J. Hydrol. 204 (1-4), 182–196. https://doi.org/10.1016/S0022-1694(97)00125-X.

Hamed, K.H., Rao, A.R., 2008. Trend detection in hydrologic data: the mann-kendall trend test under the scaling hypothesis. J. Hydrol. 204 (1), 182–196. https://doi.org/10.1016/j.jhydrol.2007.11.009.

Hardwick, S.R., Toumi, R., Pfeifer, M., Turner, E.C., Nilus, R., Ewers, R.M., 2015. The relationship between leaf area index and microclimate in tropical forest and oil palm plantation: forest disturbance drives changes in microclimate. Agr. Forest Meteorol. 201, 187–195. https://doi.org/10.1016/j.agrformet.2014.11.010.

Harris, I., Osborn, T.J., Jones, P., Lister, D., 2020. Version 4 of the cru ts monthly high-resolution gridded multivariate climate dataset. Sci. Data 7 (1). https://doi.org/10.1038/s41597-020-0453-3.

Haverd, Vanessa, Smith, Benjamin, Canadell, Josep G., Cuntz, Matthias, Mikaloff-Fletcher, Sara, Farquhar, Graham, Woodgate, William, Briggs, Peter R., Trudinger, Cathy M., 2020. Higher than expected CO_2 fertilization inferred from leaf to global observations. Global Change Biol 26 (4), 2390–2402. https://doi.org/10.1111/gcb.v26.410.1111/gcb.14950.

He, Q.N., Ju, W.M., Dai, S.P., He, W., Song, L., Wang, S.H, Li, X.C., Mao, G.X., 2021. Drought Risk of Global Terrestrial Gross Primary Productivity Over the Last 40 Years Detected by a Remote Sensing-driven Process Model. J. Geophys. Res-Biogeo. 126, e2020JG005944 https://doi.org/10.1029/2020JG005944.

Houghton, R.A., 2007. Balancing the global carbon budget. Annu. Rev. Earth Pl. Sc. 35 (1), 313–347. https://doi.org/10.1146/annurev.earth.35.031306.140057.

Huang, N., Wang, L., Song, X.P., Black, T.A., Jassal, R.S., Myneni, R.B., Wu, C.Y., Wang, L., Song, W.J., Ji, D.B., Yu, S.S., Niu, Z., 2020. Spatial and temporal variations in global soil respiration and their relationships with climate and land cover. Sci. Adv. 6 (41), eabb8508. https://doi.org/10.1126/sciadv.abb8508.

Humphrey, V., Zscheischler, J., Ciais, P., Gudmundsson, L., Sitch, S., Seneviratne, S.I., 2018. Sensitivity of atmospheric CO_2 growth rate to observed changes in terrestrial water storage. Nature 560 (7720), 628–631. https://doi.org/10.1038/s41586-018-0424-4.

Huxman, T.E., Smith, M.D., Fay, P.A., Knapp, A.K., Shaw, M.R., Loik, M.E., Smith, S.D., Tissue, D.T., Zak, J.C., Weltzin, J.F., Pockman, W.T., Sala, O.E., Haddad, B.M., Harte, J., Koch, G.W., Schwinning, S., Small, E.E., Williams, D.G., 2004. Convergence across biomes to a common rain-use efficiency. Nature 429 (6992), 651–654. https://doi.org/10.1038/nature02561.

John, T.W., Gregory, B., Zhang, L.M., Katherine, B.B., Barkley, C.S., Schwede, D.B., 2020. A review of measurements of air-surface exchange of reactive nitrogen in natural ecosystems across north america - sciencedirect. Sci. Total Environ. 698, 133975. https://doi.org/10.1016/j.scitotenv.2019.133975.

Jolly, W.M., Cochrane, M.A., Freeborn, P.H., Holden, Z.A., Brown, T.J., Williamson, G.J., Bowman, D.M.J.S., 2015. Climate-induced variations in global wildfire danger from 1979 to 2013. Nat. Commun. 6 (1) https://doi.org/10.1038/ncomms8537.

Kanakidou, M., Myriokefalitakis, S., Daskalakis, N., Fanourgakis, G., Nenes, A., Baker, A. R., Tsigaridis, K., Mihalopoulos, N., 2016. Past, Present, and Future Atmospheric Nitrogen Deposition. J. Atmos. Sci. 73 (5) https://doi.org/10.1175/JAS-D-15-0278.1.

Knapp, A.K., 2001. Variation Among Biomes in Temporal Dynamics of Aboveground Primary Production. Science 291 (5503), 481–484. https://doi.org/10.1126/science.291.5503.481.

Koster, R.D., Dirmeyer, P.A., Guo, Z.C., Bonan, G., Chan, E., Cox, P., Gordon, C.T., 2004. Regions of Strong Coupling Between Soil Moisture and Precipitation. Science 305 (5687), 1138–1140. https://doi.org/10.1126/science.1100217.

Lagler, K., Schindelegger, M., Böhm, J., Krásná, H., Nilsson, T., 2013. GPT2: Empirical slant delay model for radio space geodetic techniques. Geophys. Res. Lett. 40 (6), 1069–1073. https://doi.org/10.1002/grl.v40.610.1002/grl.50288.

Lee, E., Zeng, F.W., Koster, R.D., Weir, B., Ott, L.E., Poulter, B., 2018. The impact of spatiotemporal variability in atmospheric CO_2 concentration on global terrestrial carbon fluxes. Biogeosciences 1–32. https://doi.org/10.5194/bg-2018-187.

Liang, S.L., Zhao, X., Liu, S.H., Yuan, W.P., Cheng, X., Xiao, Z.Q., Zhang, X.T., Liu, Q., Cheng, J., Tang, H.R., Qu, Y.H., Bo, Y.C., Qu, Y., Ren, H.Z., Yu, K., Townshend, J., 2013. A long-term global land surface satellite (glass) data-set for environmental studies. Int. J. Digit. Earth 6 (sup1), 5–33. https://doi.org/10.1080/17538947.2013.805262.

Libiseller, C., Grimvall, A., 2002. Performance of partial mann-kendall tests for trend detection in the presence of covariates. Environmetrics 13 (1), 71–84. https://doi.org/10.1002/(ISSN)1099-095X10.1002/env.v13:110.1002/env.507.

Liu, X.P., Pei, F.S., Wen, Y.Y., Li, X., Wang, S.J., Wu, C.J., Cai, Y.L., Wu, J.G., Chen, J., Feng, K.S., Liu, J.G., Hubacek, K., Davis, S.J., Yuan, W.P., Yu, L., Liu, Z., 2019b. Global urban expansion offsets climate-driven increases in terrestrial net primary productivity. Nat. Commun. 10 (1) https://doi.org/10.1038/s41467-019-13462-1.

Liu, J., Rambal, S., Mouillot, F., 2015. Soil drought anomalies in modis gpp of a mediterranean broadleaved evergreen forest. Remote Sens. 7 (1), 1154–1180. https://doi.org/10.3390/rs70101154.

Liu, Z.H., Ballantyne, A.P., Poulter, B., Anderegg, W.R.L., Li, W., Bastos, A., Ciais, P., 2018. Precipitation thresholds regulate net carbon exchange at the continental scale. Nat. Commun. 9 (1) https://doi.org/10.1038/s41467-018-05948-1.

Lei, O.Y., Ping, Z., Zhu, L.W., Zhang, Z.Z., Zhao, X.H., Ni, G.Y., 2017. Difference in response of water use to evaporative demand for codominant diffuse-porous versus ring-porous tree species under N addition in a temperate forest. Ecohydrology 10 (4). https://doi.org/10.1002/eco.1829.

Zscheischler, J., Mahecha, M.D., von Buttlar, J., Harmeling, S., Jung, M., Rammig, A., Randerson, J.T., Schölkopf, B., Seneviratne, S.I., Tomelleri, E., Zaehle, S., Reichstein, M., 2014. A few extreme events dominate global interannual variability in gross primary production. Environ. Res. Lett. 9 (3), 035001. https://doi.org/10.1088/1748-9326/9/3/035001.

Liu, Z., Chen, L., Smith, N.G., Liu, Z., Chen, L., Smith, N.G., Yuan, P., Chen, X.H., Zhou, G.Y., Alam, S.A., Lin, K.R., Zhao, T.T.G., Zhou, P., Chu, C.J., Ma, H.Q., Liu., J.Q., 2019a. Global divergent responses of primary productivity to water, energy, and CO_2. Environ. Res. Lett. https://doi.org/10.1088/1748-9326/ab57c5.

Liu, Y.W., Liu, Y.B., Wang, W., Zhou, H., 2021. Propagation of soil moisture droughts in a hotspot region: Spatial pattern and temporal trajectory. J. Hydrol. 593, 125906. https://doi.org/10.1016/j.jhydrol.2020.125906.

Lu, X.H., Jiang, H., Zhang, X.Y., Liu, J.X., Zhang, Z., Jin, J.X., Wang, Y., Xu, J.H., Cheng, M.M., 2013. Estimated global nitrogen deposition using No_2 column density. Int. J. Remote Sens. 34 (24), 8893–8906. https://doi.org/10.1080/01431161.2013.853894.

Luo, Y.Q., 2007. Terrestrial carbon-cycle feedback to climate warming. Annu. Rev. Ecol. Evol. Syst. 38 (1), 683–712. https://doi.org/10.1146/annurev.ecolsys.38.091206.095808.

Ma, J., Yan, X., Dong, W., Chou, J., 2015. Gross primary production of global forest ecosystems has been overestimated. Sci. Rep-UK 5, 10820. https://doi.org/10.1038/srep10820.

Madani, N., Parazoo, N.C., Kimball, J.S., Ballantyne, A.P., Reichle, R.H., Maneta, M., Saatchi, S., Palmer, P.I I., Liu, Z.H., Tagesson, T., 2020. Recent Amplified Global Gross Primary Productivity Due to Temperature Increase Is Offset by Reduced Productivity Due to Water Constraints. AGU. Advances 1 (4). https://doi.org/10.1029/2020AV000180.

McKinnon, K.A., Poppick, A., Simpson, I.R., 2021. Hot extremes have become drier in the United States Southwest. Nat. Clim. Chang. https://doi.org/10.1038/s41558-021-01076-9.

Medlyn, B.E., Zaehle, S., De Kauwe, M.G., Walker, A.P., Dietze, M.C., Hanson, P.J., Hickler, T., Jain, A.K., Luo, Y.Q., Parton, W., Prentice, I.C., Thornton, P.E., Wang, S. S., Wang, Y.P., Weng, E.S., Iversen, C.M., McCarthy, H.R., Warren, J.M., Oren, R., Norby, R.J., 2015. Using ecosystem experiments to improve vegetation models. Nat. Clim. Chang. 5 (6), 528–534.

Nemani, R.R., 2003. Climate-Driven Increases in Global Terrestrial Net Primary Production from 1982 to 1999. Science 300 (5625), 1560–1563. https://doi.org/10.1126/science.1082750.

Peng, D.L., Zhang, B., Liu, L.Y., Fang, H.L., Chen, D.M., Hu, Y., Liu, L.L., 2012. Characteristics and drivers of global NDVI-based FPAR from 1982 to 2006. Global Biogeochem. Cycles 26 (3). https://doi.org/10.1029/2011GB004060.

Pesaresi, M., Florczyk, A., Schiavina, M., Melchiorri, M., Maffenini, L., 2019. GHS-SMOD R2019A - GHS settlement grid, updated and refined REGIO model 2014 in application to GHS-BUILT R2018A and GHS-POP R2019A, multitemporal (1975–1990-2000-2015). European Commission, Joint Research Centre (JRC). https://doi.org/10.2905/42E8BE89-54FF-464E-BE7B-BF9E64DA5218.

Pickering, C.M., Hill, W., Newsome, D., Leung, Y.F., 2010. Comparing hiking, mountain biking and horse riding impacts on vegetation and soils in Australia and the United States of America. J. Environ. Manage. 91 (3), 551–562. https://doi.org/10.1016/j.jenvman.2009.09.025.

Potter, C.S., Randerson, J.T., Field, C.B., Matson, P.A., Vitousek, P.M., Mooney, H.A., Klooster, S.A., 1993. Terrestrial ecosystem production: a process model based on global satellite and surface data. Glob. Biogeochem. Cy. 7 (4), 811–841. https://doi.org/10.1029/93GB02725.

Poulter, B., Frank, D., Ciais, P., Myneni, R.B., Andela, N., Bi, J., Broquet, G., Canadell, J. G., Chevallier, F., Liu, Y.Y., Running, S.W., Sitch, S., van der Werf, G.R., 2014. Contribution of semi-arid ecosystems to interannual variability of the global carbon cycle. Nature 509 (7502), 600–603. https://doi.org/10.1038/nature13376.

Prince, S.D., Goward, S.N., 1995. “Global Primary Production: A Remote Sensing Approach”. J. Biogeogr. 22 (4/5), 815. https://doi.org/10.2307/2845983.

Qiu, R.N., Han, G., Ma, X., Sha, Z.Y., Shi, T.Q., Xu, H., Zhang, M., 2020. CO_2 Concentration, A Critical Factor Influencing the Relationship between Solar-induced Chlorophyll Fluorescence and Gross Primary Productivity. Remote Sens. 12 (9), 1377. https://doi.org/10.3390/rs12091377.

Reichstein, M., Tenhunen, J.D., Roupsard, O., Ourcival, J.M., Rambal, S., Miglietta, F., Peressotti, A., Pecchiari, M., Tirone, G., Valentini, R., 2002. Severe drought effects on ecosystem CO_2 and H_2O fluxes at three Mediterranean evergreen sites: revision of current hypotheses? Global Change Biol 8 (10), 999–1017. https://doi.org/10.1046/j.1365-2486.2002.00530.x.

Saleska, S.R., Didan, K., Huete, A.R., da Rocha, H.R., 2007. Amazon Forests Green-Up During 2005 Drought. Science 318 (5850), 612. https://doi.org/10.1126/science.1146663.

Schwalm, C.R., Williams, C.A., Schaefer, K., Baldocchi, D., Black, T.A., Goldstein, A.H., Law, B.E., Oechel, W.C., Paw U, K.T., Scott, R.L., 2012. Reduction in carbon uptake during turn of the century drought in western North America. Nat. Geosci. 5 (8), 551–556. https://doi.org/10.1038/ngeo1529.

Sellers, P.J., Mintz, Y., Sud, Y.C., Dalcher, A., 1986. ‘A Simple Biosphere Model (SiB) for use within General Circulation Models’. J. Atmos. Sci. 43 (6), 505531. https://doi.org/10.1175/1520-0469.

Schimel, D., Stephens, B.B., Fisher, J.B., 2015. Effect of increasing CO_2 on the terrestrial carbon cycle. Proc. Natl Acad. Sci. USA 112 (2), 436–441. https://doi.org/10.1073/pnas.1407302112.

Schwalm, C.R., Anderegg, W.R.L., Michalak, A.M., Fisher, J.B., Biondi, F., Koch, G., Litvak, M., Ogle, K., Shaw, J.D., Wolf, A., Huntzinger, D.N., Schaefer, K., Cook, R., Wei, Y.X., Fang, Y.Y., Hayes, D., Huang, M.Y., Jain, A., Tian, H.Q., 2017. Global patterns of drought recovery. Nature 548 (7666), 202–205. https://doi.org/10.1038/nature23021.

Schwalm, C.R., Huntzinger, D.N., Michalak, A.M., Schaefer, K., Fisher, J.B., Fang, Y.Y., Wei, Y.X., 2020. Modeling suggests fossil fuel emissions have been driving increased land carbon uptake since the turn of the 20th century. Sci. Rep.-UK 10 (1). https://doi.org/10.1038/s41598-020-66103-9.

Schuur, E.A.G., 2003. Productivity and global climate revisited: the sensitivity of tropical forest growth to precipitation. Ecology 84, 1165–1170. https://doi.org/10.1890/0012-9658(2003)084[1165:PAGCRT]2.0.CO;2.

Stocker, B.D., Zscheischler, J., Keenan, T.F., Prentice, I.C., Seneviratne, S.I., Peñuelas, J., 2019. Drought impacts on terrestrial primary production underestimated by satellite monitoring. Nat. Geosci. https://doi.org/10.1038/s41561-019-0318-6.

Stocker, B.D., Zscheischler, J., Keenan, T.F., Prentice, I.C., Peñuelas, J., Seneviratne, S.I., 2018. Quantifying soil moisture impacts on light use efficiency across biomes. New Phytol. 218 (4), 1430–1449. https://doi.org/10.1111/nph.15123.

Sun, Z.Y., Wang, X.F., Yamamoto, H., Tani, H., Zhong, G.S., Yin, S., Guo, E.L., 2018. Spatial pattern of GPP variations in terrestrial ecosystems and its drivers: Climatic factors, CO_2 concentration and land-cover change, 1982–2015. Ecol. Inform. 46, 156–165. https://doi.org/10.1016/j.ecoinf.2018.06.006.

Sun, Z.Y., Wang, X.F., Zhang, X.R., Tani, H., Guo, E.L., Yin, S., Zhang, T.Y., 2019. Evaluating and comparing remote sensing terrestrial gpp models for their response to climate variability and CO_2 trends. Sci. Total Environ. 668, 696–713. https://doi.org/10.1016/j.scitotenv.2019.03.025.

Tang, A.M., Hughes, P.N., Dijkstra, T.A., Askarinejad, A., Brencic, M., Cui, Y.J., Diez, J.J., Firgi, T., Gajewska, B., Gentile, F., Grossi, G., Jommi, C., Kehagia, F., Koda, E., ter-Maat, H.W., Lenart, S., Lourenco, S., Oliveira, M., Osinski, P., Springman, S.M., Stirling, R., Toll, D.G., Van, B.V., 2018. Atmosphere–vegetation–soil interactions in a climate change context; impact of changing conditions on engineered transport infrastructure slopes in Europe. Q. J. Eng. Geol. Hydroge. qjegh2017-103. https://doi.org/10.1144/qjegh2017-103.

Templer, P.H., Pinder, R.W., Goodale, C.L., 2012. Effects of nitrogen deposition on greenhouse-gas fluxes for forests and grasslands of North America. Front. Ecol. Environ. 10 (10), 547–553. https://doi.org/10.1890/120055.

Tian, S.Y., Renzullo, L.J., Dijk, A.I.J.M.V., Tregoning, P., Walker, J.P., 2019. Global joint assimilation of grace and smos for improved estimation of root-zone soil moisture and vegetation response. Hydrol. Earth Syst. Sc.23(2), 1067–1081. https://doi.org/10.5194/hess-23-1067-2019.

Van, S.E., Killaars, L., Smith, N.E., Koren, G., van Beek, L.P.H., Peters, W., van der Laan-Luijkx, I.T., 2018. Changes in surface hydrology, soil moisture and gross primary production in the Amazon during the 2015/2016 El Niño. Philos. T. R. Soc. B. 373 (1760), 20180084. https://doi.org/10.1098/rstb.2018.0084.

Veldkamp, T.I.E., Wada, Y., Aerts, J.C.J.H., Ward, P.J., 2016. Towards a global water scarcity risk assessment framework: incorporation of probability distributions and hydro-climatic variability. Environ. Res. Lett. 11 (2), 024006. https://doi.org/10.1088/1748-9326/11/2/024006.

Vuichard, N., Messina, P., Luyssaert, S., Guenet, B., Zaehle, S., Ghattas, J., Bastrikov, V., Peylin, P., 2019. Accounting for carbon and nitrogen interactions in the global terrestrial ecosystem model orchidee (trunk version, rev 4999): multi-scale evaluation of gross primary production. Geosci. Model Dev. 12 (11), 4751–4779. https://doi.org/10.5194/gmd-12-4751-2019.

Walcek, C.J., Brost, R.A., Chang, J.S., Wesely, M.L., 1986. SO_2, Sulfate and HNO_3 Deposition Velocities Computed Using Regional Landuse and Meteorological Data. Atmos. Environ. 20 (5), 949–964. https://doi.org/10.1016/0004-6981(86)90279-9.

Wan, Z.M., 2015. University of California Santa Barbara, Simon Hook, Glynn Hulley - JPL and MODAPS SIPS - NASA. MYD11C3 MODIS/Aqua Land Surface Temperature and the Emissivity Monthly L3 Global 0.05Deg CMG. NASA LP DAAC. doi:10.5067/MODIS/MYD11C3.006.

Wang, M., Sun, R., Zhu, A., Xiao, Z., 2020a. Evaluation and comparison of light use efficiency and gross primary productivity using three different approaches. Remote Sens. 12 (6), 1003. https://doi.org/10.3390/rs12061003.

Wang, S.H., Zhang, Y.G., Ju, W.M., Chen, J.M., Ciais, P., Cescatti, A., et al., 2020b. Recent global decline of CO_2 fertilization effects on vegetation photosynthesis. Science 370 (6522), 1295–1300. https://doi.org/10.1126/science:abb7772.

Wang, M.M., Wang, S.Q., Zhao, J., Ju, W.M., Hao, Z., 2021. Global positive gross primary productivity extremes and climate contributions during 1982–2016. Sci. Total Environ. 774, 145703. https://doi.org/10.1016/j.scitotenv.2021.145703.

Williams, I.N., Torn, M.S., Riley, W.J., Wehner, M.F., 2014. Impacts of climate extremes on gross primary production under global warming. Environ. Res. Lett. 9 (9), 094011. https://doi.org/10.1088/1748-9326/9/9/094011.

Wesely, M.L., 2007. Parameterization of surface resistances to gaseous dry deposition in regional-scale numerical models. Atmos. Environ. 41, 52–63. https://doi.org/10.1016/j.atmosenv.2007.10.058.

Wieder, W.R., Cleveland, C.C., Smith, W. Kolby, Todd-Brown, K., 2015. Future productivity and carbon storage limited by terrestrial nutrient availability. Nat. Geosci. 8 (6), 441–444. https://doi.org/10.1038/ngeo2413.

Xu, C.G., McDowell, N.G., Fisher, R.A., Wei, L., Sevanto, S., Christoffersen, B.O., Weng, E. S., Middleton, R.S., 2019. Increasing impacts of extreme droughts on vegetation productivity under climate change. Nat. Clim. Change 9 (12), 948–953. https://doi.org/10.1038/s41558-019-0630-6.

Yao, J.Y., Liu, H.P., Huang, J.P., Gao, Z.M., Wang, G.Y., Li, D., Yu, H.P., Chen, X.Y., 2020. Accelerated dryland expansion regulates future variability in dryland gross primary production. Nat. Commun. 11 (1) https://doi.org/10.1038/s41467-020-15515-2.

Yu, T., Sun, R., Xiao, Z.Q., Zhang Q., Wang, J.M., Liu, G., 2018a. Generation of high resolution vegetation productivity from a downscaling method. Remote Sens. 10 (11). https://doi.org/10.3390/rs10111748.

Yu, T., Sun, R., Xiao, Z., Zhang, Q., Liu, G., Cui, T., Wang, J., 2018b. Estimation of Global Vegetation Productivity from Global LAnd Surface Satellite Data. Remote Sens. 10 (2), 327. https://doi.org/10.3390/rs10020327.

Zheng, Y., Zhang, L., Xiao, J.F., Yuan, W.P., Yan, M., Li, T., Zhang, Z.Q., 2018. Sources of uncertainty in gross primary productivity simulated by light use efficiency models: model structure, parameters, input data, and spatial resolution. Agr. Forest Meteorol. 263, 242–257. https://doi.org/10.1016/j.agrformet.2018.08.003.

Yuan, W.P., Cai, W.W., Chen, Y., Liu, S.G., Dong, W.J., Zhang, H.C., Yu, G.R., Chen, Z.Q., He, H.L., Guo, W.D., Liu, D., Liu, S.M., Xiang, W.H., Xie, Z.H., Zhao, Z.H., Zhou, G. M., 2016. Severe summer heatwave and drought strongly reduced carbon uptake in Southern China. Sci. Rep-UK 6 (1). https://doi.org/10.1038/srep18813.

Zhang, Y., Xiao, X.M., Guanter, L., Zhou, S., Ciais, P., Joiner, J., Sitch, S., Wu, X.C., Nabel, J., Dong, J.W., Kato, E., Jain, A.K., Wiltshire, A., Stocker, B.D., 2016. Precipitation and carbon-water coupling jointly control the interannual variability of global land gross primary production. Sci. Rep-UK 6 (1). https://doi.org/10.1038/srep39748.

Zhang, Y., Xiao, X.M., Wu, X.C., Zhou, S., Zhang, G., Qin, Y.W., Dong, J.W., 2017. A global moderate resolution dataset of gross primary production of vegetation for 2000–2016. Sci. Data 4, 170165. https://doi.org/10.1038/sdata.2017.165.

Zhang, Y.J., Yu, G.R., Yang, J., Wimberly, M.C., Zhang, X.Z., Tao, J., Jiang, Y.B., Zhu, J. T., 2014. Climate-driven global changes in carbon use efficiency. Global Ecol. and Biogeogr. 23 (2), 144–155. https://doi.org/10.1111/geb.2014.23.issue-210.1111/geb.12086.

Zhao, M., Running, S.W., Nemani, R.R., 2006. 'Sensitivity of Moderate Resolution Imaging Spectroradiometer (MODIS) Terrestrial Primary Production to the Accuracy of Meteorological Reanalyses'. J. Geophys. Res. 111, (G1). https://doi.org/10.1029/2004JG000004.

Zhu, P., Zhuang, Q., Ciais, P., Welp, L., Li, W., Xin, Q., 2017. Elevated atmospheric CO_2 negatively impacts photosynthesis through radiative forcing and physiology-mediated climate feedback. Geophys. Res. Lett. 44 (4) https://doi.org/10.1002/2016gl071733.